Optical measurements of a lcv-combustor operated in a micro gas turbine with various fuel compositions

Timo Zornek*

German Aerospace Center (DLR)
Institute of Combustion Technology
Pfaffenwaldring 38-40
70569 Stuttgart, Germany
Email: timo.zornek@dlr.de

Thomas Mosbach

German Aerospace Center (DLR)
Institute of Combustion Technology
Pfaffenwaldring 38-40
70569 Stuttgart, Germany

Manfred Aigner

German Aerospace Center (DLR)
Institute of Combustion Technology
Pfaffenwaldring 38-40
70569 Stuttgart, Germany

ABSTRACT

In a recent joint research project, a new FLOX®-combustion system was developed to couple a fixed-bed gasifier with a micro gas turbine. Product gases from biomass gasification exhibit low calorific values and varying compositions of mainly H_2, CO, CO_2, N_2 and CH_4. Furthermore, combustion characteristics differ significantly compared to the commonly used natural gas. As the FLOX®-technology is considered as efficient and fuel-flexible featuring low emissions of hazardous pollutants, the design of the LCV-combustor is based on it. It contains a two-staged combustor consisting of a jet-stabilized main stage adapted from the FLOX®-concept combined with a swirl stabilized pilot stage. The combustor was operated in a Turbec T100 test rig using an optically accessible combustion chamber, which allowed OH-chemiluminescence and OH-PLIF measurements for various fuel compositions. In particular, the hydrogen content in the synthetically mixed fuel gas was varied from 0 % to 30 %. The exhaust gas composition was additionally analysed regarding CO, NO_x and unburned hydrocarbons. The results provide a comprehensive insight into the flame behaviour during turbine operation. Efficient combustion and stable operation of the micro gas turbine was observed for all fuel compositions, while the hydrogen showed a strong influence. It is remarkable, that with hydrogen contents higher than 9 % no OH radicals were detected within the inner recirculation zone, while they were increasingly entrained below hydrogen contents of 9 %. Without hydrogen, the inner recirculation zone was completely filled with OH radicals and the highest concentrations were detected there. Therefore, the results indicate a different flame behaviour with low and high hydrogen contents. Although the flame shape and position was affected, pollutant emissions remained consistent below 10 ppm based on 15 % O_2. Only in case of 0 % hydrogen, CO-emissions increased to 43 ppm, which is still meeting the emission limits. Thus, the combustor allows operation with syngases having hydrogen contents from 0 % to 30 %.*

INTRODUCTION

Micro gas turbines (MGT) constitute an upcoming technology in the field of decentralized combined heat and power (CHP) production [1]. It offers various advantages such as low maintenance requirements, low vibrations, high fuel-flexibility as well as low emissions [2]. The latter is facilitated by the stationary combustion in micro gas turbines, which

*Address all correspondence to this author.

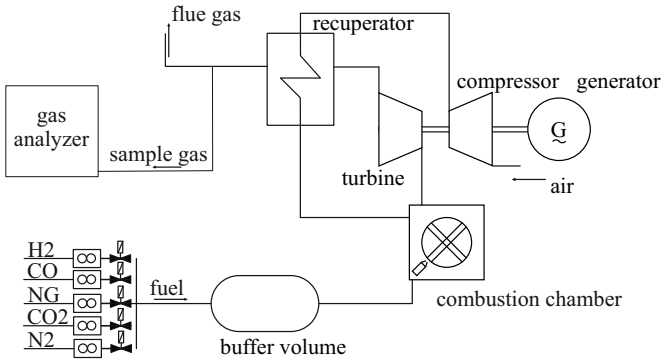

Fig. 1: SCHEMATIC OF THE TEST RIG [5].

enables meeting emission limits without additional exhaust gas after treatment. Due to the supposed high fuel-flexibility, there is a growing interest in using alternative fuels in MGTs [3]. However, the combustors of most commercial MGTs are designed for conventional fuels like natural gas, which exhibit high calorific values.

In contrast to natural gas, product gases from fixed-bed gasification of biomass exhibit lower calorific values (LCV) of only 3.5 MJ/kg to 5 MJ/kg [4], which is about 10 % of the LCV of natural gas. High fuel mass flows are the consequence, which change the momentums within the combustion chamber and require greater flow cross sections and fuel valves. Additionally, important combustion characteristics like flame velocity and ignition delays depend strongly on the fuel composition. Hence, the current combustion systems of commercial MGTs are often not suitable to operate with LCV fuels. Furthermore, the significantly higher fuel mass flow rates lead to shifted operating points of components like compressor and power electronic, which might limit operation of some MGTs [5].

Regarding the use of LCV-fuels in gas turbine combustors, there is a lot of work being done. Beside common swirl combustors, there are recently some promising new technologies such as the FLOX® [6], which operate with high preheated air. Similar approaches are MILD combustion [7], colourless combustion (CDC) [8] and High Temperature Air Combustion (HiTAC) [9]. The FLOX® technology is considered to be fuel-flexible while exhibiting low pollutant emissions, low risk of flashback, low risk of combustion instabilities and pressure loses below 5 % [10–12]. Although FLOX® combustors are already applied in industrial furnaces, they are still at the level of prototypes for gas turbine applications [13]. Some prototypes have been successfully operated in micro gas turbines by Zanger et al. [14] and Zornek et al. [5].

In the present paper, the FLOX®-combustor, which was designed for LCV fuels and successfully operated in the micro gas turbine by Zornek et al. [5], was implemented into an optical accessible combustion chamber in order to analyse the influence of the hydrogen contained in the fuel. In literature, hydrogen is reported to be predominant for the chemical reaction of product gases and its characteristics like flame speed and ignition delay time [15, 16]. Therefore, the amount of hydrogen contained in the fuel has a significant impact on flame stabilization as well as on emissions.

Some fuels like blast furnace gas are similar to product gases but exhibit low concentrations of hydrogen. On the other side, product gases from steam gasification reach high amounts of hydrogen. By varying the hydrogen content of the fuel, this work also investigates the ability of the used combustor to operate with different types of LCV-fuels. The MGT was fed using a synthetic fuel supply system to vary the composition during operation. OH*-chemiluminescence and OH-PLIF measurements were conducted to evaluate combustion qualitatively. An exhaust gas analysis system delivered the concentrations of pollutant emissions and information about combustion efficiency.

EXPERIMENTAL SETUP

Micro gas turbine test rig

The LCV-combustor has been operated in a MGT test rig, which is schematically presented in Fig. 1. The MGT used is a Turbec T100 PH series 3 with a nominal electrical power output of 100 kW_{el}. Turbine, compressor and generator are mounted on a single shaft. The radial compressor delivers the pressurized process air with a pressure ratio of 4.5. Before entering the combustion chamber, the air is heated up by compression and by an additional recuperator to more than 600 °C. Due to the mixing with dilution air, the exhaust gas enters the radial turbine with a maximum inlet temperature of 950 °C, which is limited by the material of the turbine and the recuperator. By expansion, the exhaust gas cools down to 645 °C and passes through the recuperator. There, heat is transferred to the incoming process air and the exhaust gas leaves the recuperator with about 270 °C. During the experiments, a fraction of the exhaust gas was led to an exhaust gas analysis system, which contains the analysers listed in Table 1.

At the test rig, the T100 was fed by a synthetic fuel consisting of hydrogen, carbon monoxide, carbon dioxide, nitrogen

Table 1: ABB EXHAUST GAS ANALYSIS SYSTEM

Analyser	Species	Range	Accuracy
MAGNOS 206	O_2	0...25 Vol%	±0,125 Vol%
URAS 26	CO	0...50 ppm	±0,5 ppm
	CO_2	0...5 Vol%	±0,05 Vol%
LIMAS 11HW	NO	0...10 ppm	±0,1 ppm
	NO_2	0...10 ppm	±0,1 ppm
MULTI FID14	C	0...10 ppm	±0,1 ppm

and natural gas. The fuel supply system controlled the pressure in a buffer volume, where the components were mixed together. Separate flow controllers for each component ensured the required ratios. The overall fuel mass flow was determined by the consumption of the turbine and calculated by the sum of the flow controllers measurement values. The set-up allowed the variation of the fuel composition while running the turbine.

Combustor design

The combustor used in this work was designed for the operation of the Turbec T100 with low calorific fuels. Figure 2 shows a schematic of the combustion chamber while Fig. 3 shows a picture of the manufactured prototype. The preheated air is divided into combustion and dilution air. The latter constitutes about two third of the total air flow and is used to cool down the exhaust gas temperature to the maximum allowed turbine inlet temperature. The combustion air streams along the liner, where it is additionally heated up before it turns around to enter the two-staged combustor. The swirl stabilized pilot stage is recessed in the centre of the combustor. Fuel and air are partially premixed before entering the combustion chamber of the pilot stage. The hot exhaust gases from the pilot stage support the subsequent main stage. The latters design is adopted from FLOX®-combustors and exhibits ten annular arranged air nozzles, where the fuel is injected coaxially. A central recirculation zone, generated by the momentum of the axial jets, stabilizes combustion by mixing hot exhaust gases with the entraining mixture of fuel and air.

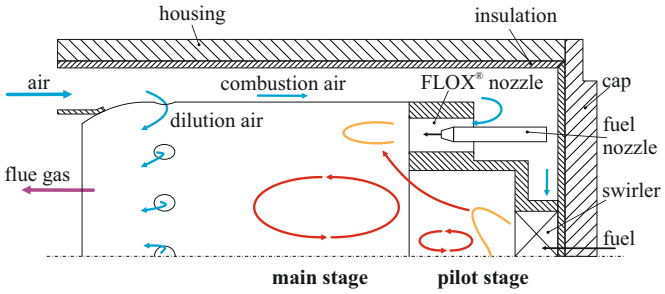

Fig. 2: SCHEMATIC OF THE COMBUSTION CHAMBER [5].

Set-up for optical measurement

In order to investigate combustion while operating the micro gas turbine, an optically accessible combustion chamber shown in Fig. 4 was added to the Turbec T100. It contained a square cross section and exhibited quartz glass windows on each side, which allowed the optical access, in particular to the combustion zone of the main stage. The size of the windows was 150 x 136 mm. Due to the windows, the liner contained a square base in the optical accessible part and turned into the circular cross section of the Turbec T100 liner afterwards. The square part and the windows of the liner were cooled by pressurized air. Construction reasons required to enlarge the distance between the combustor front plate and the dilution holes about the factor 1.5 as well as the distance between dilution holes and turbine inlet. Therefore, operational conditions inside the combustion chamber changed. For instance, higher heat losses increased the fuel demand and this led to lower air numbers. The latter is here defined as the ratio of the combustion air mass flow rate to the stoichiometric air mass flow rate. Despite the mentioned deviations, the set-up enabled a comprehensive insight into the combustion behaviour.

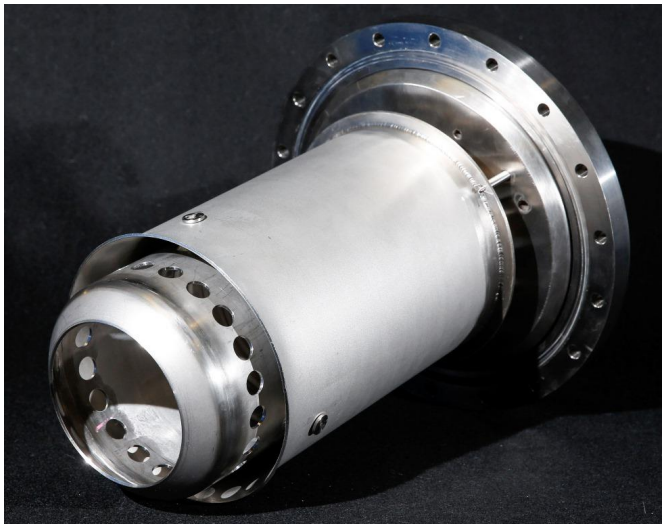

Fig. 3: COMBUSTOR PROTOTYPE (PICTURE: DLR/ FRANK EPPLER).

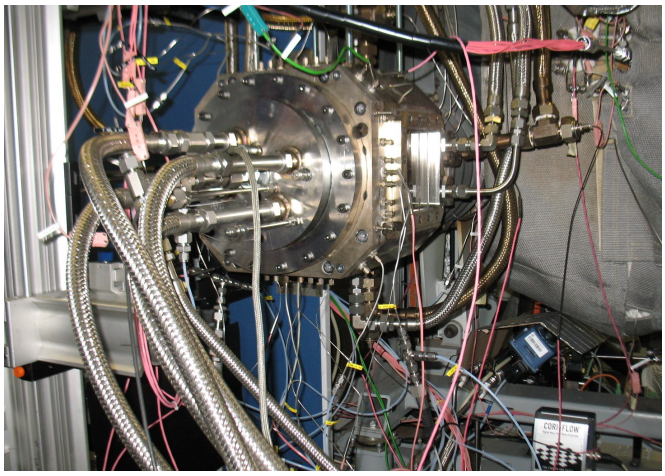

Fig. 4: OPTICAL COMBUSTION CHAMBER.

The laser system used for acquiring the OH PLIF images consists of a frequency-doubled-flash-lamp pumped Nd:YAG laser (Spectra-Physics PIV-400-10) pumping a tunable dye laser (Sirah Precision Scan, dye Rhodamine 6G) at 10 Hz repetition rate. After frequency doubling, the desired UV laser pulses for OH excitation with pulse duration of 7 ns, bandwidth of 0.4 cm^{-1}, and pulse energy of approximately 20 mJ were generated. The dye laser was tuned to the $Q_1(8)$ transition at 283.636 nm within the vibrational band v"=0, v'=1 of the OH $A2\sum E^{+} - X^2\Pi$ band system. The population of the laser-coupled ground state of the selected line varied in the temperature range between 1400 K and 2200 K by approximately 9 %. A set of cylindrical lenses in a telescopic arrangement was used to expand the circular laser beam cross-section into a light sheet with 146 mm in width. An additional cylindrical lens was used to reduce the sheet thickness to approximately 0.5 mm inside the combustion chamber. The laser sheet was deflected by a dielectric mirror vertically through the combustor. The measurement plane was oriented perpendicularly to the nozzle exit plate and vertically aligned to the axis of two air nozzles as illustrated in Fig. 5. The laser-induced OH fluorescence near 310 nm originating from the v'=1, v"=1 and v'=0, v"=0 bands was recorded perpendicular to the laser sheet by an intensified camera system (an image intensifier IRO 25 lens-coupled to a sCMOS camera purchased from LaVision). The image intensifier gate was set to 100 ns. The fluorescence was imaged with a Halle UV-lens (f/2.0, f =100 mm) through a narrow bandpass, high-transmission interference filter and a broad bandpass Schott UG 11 filter. A small portion of the laser sheet was deflected by means of a beam splitter into a quartz cell filled with fluorescent dye solution in order to correct for non-uniformities and fluctuations in the intensity of the laser sheet profile. The laser-induced fluorescence profile was simultaneously imaged to the OH-PLIF by a CCD camera (Imager Intense 3 purchased from LaVision) equipped with a common Nikon Nikkor lens (f/1.2, f=50 mm) for the visible spectral range.

The camera system and filter combination as described for the OH-PLIF measurements was also applied for imaging

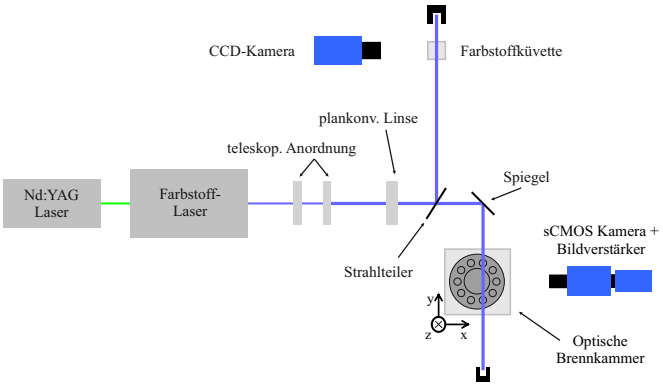

Fig. 5: SET-UP FOR OPTICAL MEASUREMENTS.

the natural flame OH* chemiluminescence. Only the image intensifier gate was changed to 50 µs and the PLIF laser was blocked.

Operating conditions

The experiments were performed at a constant rotational speed of 57750 rpm, which corresponds to 82,5 % of the maximum rotational speed of the Turbec T100. Furthermore, the turbine outlet temperature was kept at 645 °C. Due to the heat losses of the optical combustion chamber, the inlet temperature of the combustion air varied between 510 °C to 560 °C. In the configuration without optical combustion chamber the inlet temperature usually reaches 600 °C to 650 °C. At this load point, the pressure inside the combustion chamber was about 2.8 bar and the thermal power reached 260 kW, from which 7 % was introduced into the pilot stage. The global air number including dilution air was about 7.3 in this case. Assuming that 1/3 of the air is participating in combustion, the adiabatic flame temperature ranged from about 1600 K to 1700 K.

Table 2: OPERATED FUEL COMPOSITIONS IN VOL% AND LAMINAR FLAME SPEED S_u IN M/S.

H_2	CO	CH_4	CO_2	N_2	S_u
30	10	1	12	47	1.78
21	21.9	1	12	44.1	1.43
18	22	2.25	12	45.75	1.24
15	17.6	5	12	50.4	0.95
12	19	6	12	51	0.87
9	14	9	12	56	0.67
6	18	9	12	55	0.68
3	21	9	12	55	0.64
0	19	11	12	58	0.56

Table 2 presents the operated fuel compositions including the stoichiometric laminar flame speed, which gives an impression of the reactivity across this range of fuel mixtures. For its calculation the detailed reaction model of Li et. al [17] was used. Herzler et. al [15] demonstrated the ability of this reaction model to predict laminar flame speeds and ignition delay times of syngas from biomass gasification under similar conditions. A combustion air temperature of 600 °C was assumed as well as a fuel temperature of 50 °C, which has been measured in the fuel plenum of the main stage. The experiments focused on the amount of hydrogen contained in the fuel. It was varied between 0 % and 21 % in steps of 3 percentage points while the lower heating value was kept constant at 5 MJ/kg. Additionally, 30 % was measured to cover higher hydrogen concentrations like in product gases from steam gasification. The thermal power remained constant as well as the mass flows of fuel and air through the combustor. The fuel mixtures of 15 % H_2 to 21 % H_2 are typical for air blown fixed-bed gasifiers [4], which

are mostly used in small scale applications. They have been successfully operated without optical combustion chamber by Zornek et al. [5] and therefore, they were chosen as a reference.

RESULTS

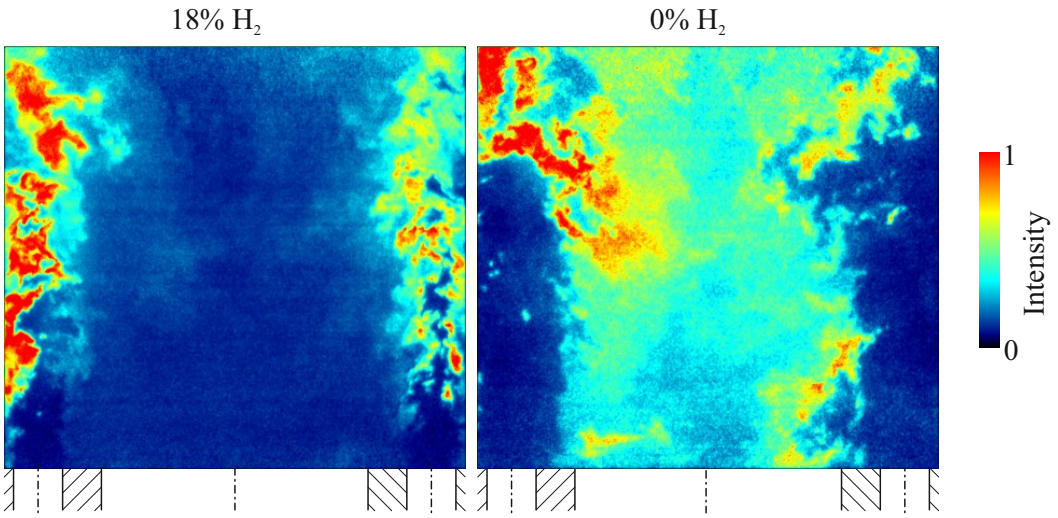

Fig. 6: INSTANTANEOUS IMAGES OF THE MEASURED OH DISTRIBUTION

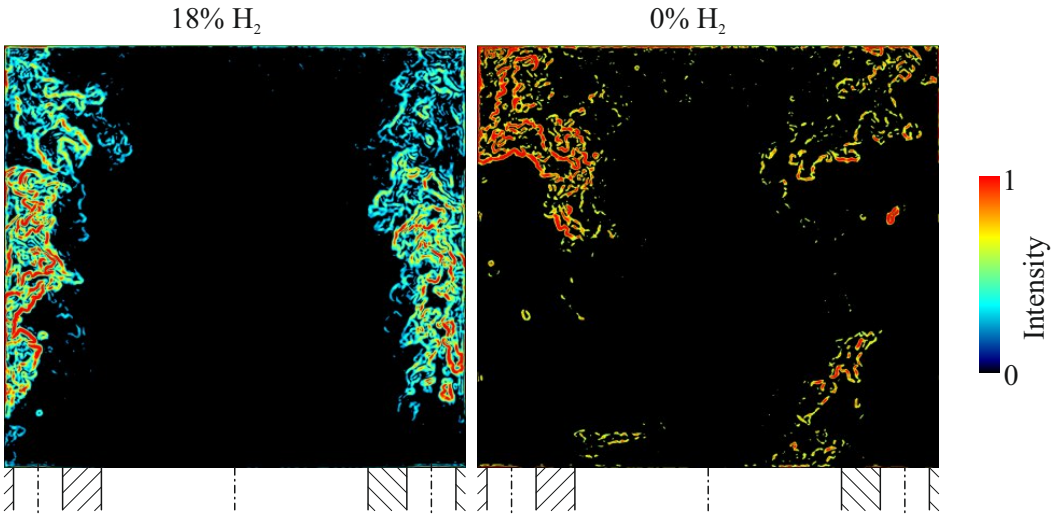

Fig. 7: ANALYSED GRADIENTS OF INSTANTANEOUS OH-PLIF IMAGES

OH*-Chemiluminescence and OH-PLIF were measured for qualitative analysis of combustion. Two instantaneous OH-PLIF images are shown in Fig. 6, one is representative for higher hydrogen concentrations and one for lower. The images depict the local distribution of OH radicals in the measurement plane, which was extended through two main stage nozzles. Their positions as well as the pilot stage are illustrated at the bottom. The images have been rotated by 90, thus the flow direction is bottom up. As the laser beam entered the combustion chamber from the left side and it was weakened within the combustion chamber, the excitation of the OH radicals decreased from left to right. Therefore, the measured intensities on the left side are higher. The images were normalized independently to their maximum intensity. The two images demonstrate a different flame behaviour. In case of 18 % H_2, OH radicals are concentrated along the main stage nozzle axis. The beginning of their formation is located closely to the nozzles orifices. It is remarkable, that the concentration of OH radicals in the

inner recirculation zone is low. This signifies that they are consumed before they can be recirculated. On the other hand, the temperature along the nozzle axis is significantly higher than in the recirculation zone. In case of 0 % H_2, the jets of the unburned mixture of fuel and air enter the combustion chamber widely. OH radicals are formed far away from the nozzles and highly entrained into the inner recirculation zone, which is completely filled. This indicates a more homogeneous temperature distribution than in the other case.

The OH-PLIF measurements provide a qualitative distribution of the OH radicals in the plane of measurement. OH radicals are usually formed in reaction zones in super-equilibrium concentrations and consumed during combustion, but they can also be present at temperatures higher than 1400 K. The equilibrium concentration increases exponentially with temperature [18]. Therefore, it is difficult to distinguish between reaction zones and areas of high temperature without chemical reactions. As OH radicals are formed quickly in a thin flame front, high gradients of OH are considered to identify reaction zones. The gradients deduced from the instantaneous OH-PLIF images shown in Fig. 6 are presented in Fig. 7. In case of 0 % H_2, there are reaction zones on the nozzle axis as well as entrained into the inner recirculation zone. The reactions take place further downstream of the combustor. This behaviour is similar to results reported by Zanger [19] for a natural gas FLOX®-combustor under lean conditions. For increasing air numbers from 2 to 3, he reported a transition of the combustion regime from wrinkled flames to thick flames (distributed combustion) as classified by Borghi [20]. Additionally, flame structures are visible for 0 % H_2, which are coming out of the pilot stage. This indicates an upstream flame position of the pilot.

Figure 6 and 7 only showed an instantaneous distribution of OH radicals and reaction zones. In order to identify the regions where they are mainly located, the averaged images of OH*-chemiluminescence, OH-PLIF and OH-PLIF gradients are presented in Fig. 8 for various fuel compositions. During steady-state operation of the turbine, 300 images of OH*-chemiluminescence and 500 images of OH-PLIF were taken. Each image is normalized separately to the maximum intensity. The results for 30 %, 15 % and 9 % to 0 % hydrogen are presented with decreasing hydrogen contents from top down. The results between 30 % and 9 % showed only marginal differences, therefore not all of them are shown here. The positions of the main stage nozzles are illustrated at the bottom of Fig. 8. The images of the OH*-chemiluminescence are larger than the OH-PLIF images due to the size of the laser beam. The upper corners in the OH*-chemiluminescence images remained black, because these areas of the image sensor have not been illuminated by the smaller image intensifier.

The images of the OH*-chemiluminescence are presented in the left column of Fig. 8. Five separate jet flames are visible between 30 % and 15 % stabilizing close to the combustor. The flame shape appears narrow and elongated with the highest intensities located in a small distance to the combustor. Looking at the three single flames of the left side, flame stabilization occurs closer to the combustor on the left than on the right side of the flames. In contrast, the two flames on the right side stabilize closer to the combustor on their right side. For the four non centric flames this can be explained by the fact, that flow velocities are slower close to the wall, where also hot exhaust gases are present. Both enhances a closer stabilisation of the reaction zones near the wall. For this reason, the measured intensity of the centric flame should be evenly distributed, which is not the case. The centric flame stabilizes closer to the combustor on the left than the right side which cannot be explained by the difference due to the wall and the inner recirculation zone. This might be caused by an uneven flow distribution of the air coming to the combustion chamber.

Only low intensities were measured at the top of the image, indicating combustion is mainly completed within the examined region. With decreasing hydrogen contained in the fuel, the flames start to lift off the combustor due to lower flame speeds and higher ignition delays with decreasing hydrogen content. Furthermore, the reaction zones become shorter and wider, and the OH*-chemiluminescence signal overlaps increasingly until the reaction zones seem to merge into two wide reaction zones. Due to the expanded reaction zones, the OH*-chemiluminescence signals overlap especially at the combustor sides, where the visible distances between the nozzles appear shorter according to the angle of the camera. Thus, the signals of four nozzles overlap and therefore, the intensity between the outer nozzles is higher than in the centre of the image. At 0 % H_2, the reaction zone in the centre disappears and seems to merge to the reaction zone on the left side of the image. This also indicates an uneven flow distribution of the air due to the construction of the micro gas turbine.

The averaged images of the OH-PLIF signal are shown in the second column of Fig. 8. Compared to the images of the OH*-chemiluminescence, only the sectional plane through two outer flames can be seen. The images represent areas, where high concentrations of OH radicals are present. With hydrogen contents higher 9 %, high concentrations of OH are found along the nozzles axis. The beginning of the OH formation is close to the exit of the nozzles and there is a sharp transition to the inner recirculation zone. With hydrogen contents below 9 %, OH radicals are increasingly entrained into the inner recirculation zone. The latter is completely filled with OH and the highest concentrations are located there for 0 %H_2 in the fuel. Hence, the areas with high OH concentrations change significantly with the amount of hydrogen.

Based on the averaged images of the OH-PLIF signals it is not possible to recognize the reaction zones within the plane of measurement. For this purpose the right column of Fig. 8 shows the averaged gradients, which were obtained from the instantaneous OH-PLIF gradient images. The gradients represent the locations of the reaction zones. In contrast to Fig. 6 and 7, these pictures indicate that combustion mainly takes place along the axis of the main stage nozzles even for low hydrogen contents, though located further downstream and much wider. In particular, the transition from higher to lower gradients becomes wider, perpendicular to the nozzle axis. Without hydrogen, the reaction zones reach into the inner recirculation

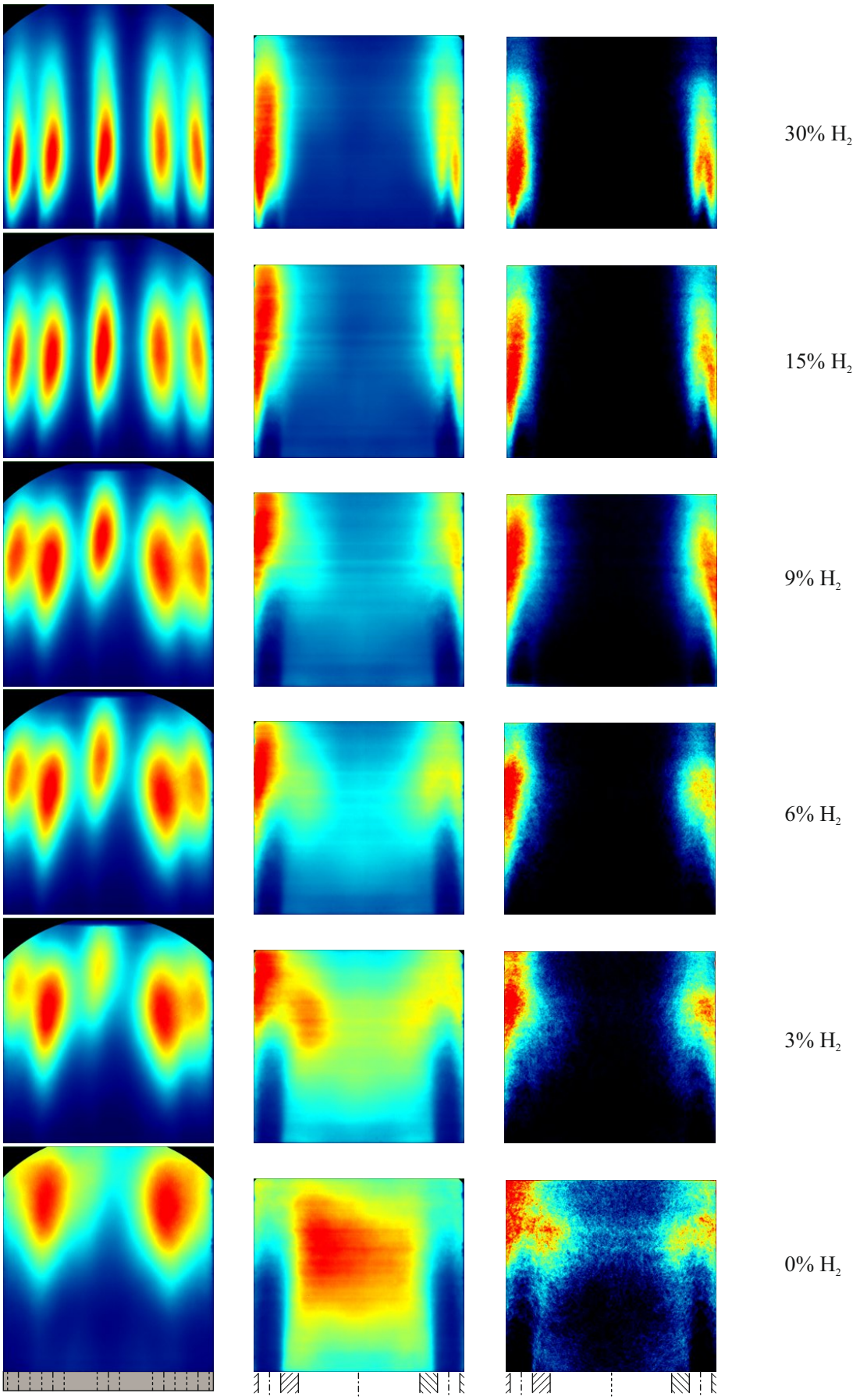

Fig. 8: AVERAGED IMAGES OF OH*-CHEMILUMINESCENCE (LEFT), OH-PLIF (CENTRE) AND OH-PLIF GRADIENTS (RIGHT)

zone. Furthermore, reacting areas coming out from the pilot stage were observed. This indicates a pilot flame, which moves downstream with lower hydrogen contents. The chemical reaction becomes to slow that the flames can stabilize close to the nozzle orifices, but combustion seems to be stabilized by the high amount of OH radicals, which are recirculated by the inner recirculation zone. The comparison between the gradients and the OH*-chemiluminescence shows good agreement, which confirms the obtained information.

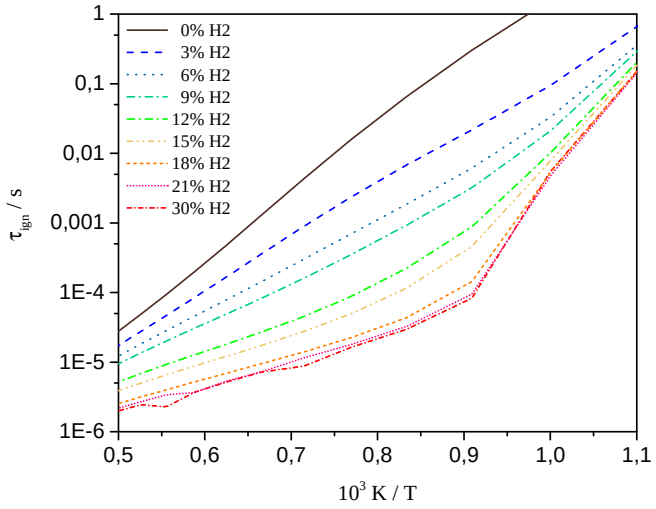

Fig. 9: IGNITION DELAY OF FUEL MIXTURES

Figure 8 demonstrates significant changes below 6 % of H_2 and marginal effects for higher concentrations although the laminar flame speed in Table 2 shows the opposite behaviour. It is only slightly increasing from 0.56 m/s to 0.67 m/s for 0 % H_2 and 9 % H_2 respectively, while it reaches 1.78 m/s for 30 % of H_2. According to the higher reactivity of the hydrogen rich fuel mixtures, a different behaviour would be expected. In order to understand the impact of H_2 on the ignition delay time, it has been calculated with the reaction model of Li et al. [17] for the various fuel compositions. The results are plotted versus the reciprocal temperature in Fig. 9. In the temperature region of 900 K to 1100 K, which is relevant for the entering mixture of fuel and air, ignition delay times decrease severely by the addition of small amounts of hydrogen. For higher concentrations of H_2, the influence on the ignition delay times of the mixtures decreases. This indicates that the combustors flame behaviour is strongly affected by the ignition delay time of the fuel.

The optical measurements indicate a different flame stabilization depending on the hydrogen content and show a lift-off flame. Usually this effects the amount of pollutant emissions. Therefore, the concentrations of carbon monoxides, nitrogen oxides and unburned hydrocarbons have been measured with 2 Hz for 15 minutes at each operating point. The averaged values are normalized to an oxygen concentration of 15 % within the dry exhaust gas and presented in Fig. 10. Remarkably, the graph shows efficient and clean combustion for all fuel compositions. Pollutant emissions change only marginally for hydrogen amounts from 30 % to 3 %. Only without hydrogen present in the fuel, the emissions of carbon monoxides and unburned hydrocarbons increase visibly. However, the concentrations remain below German emission limits for gas turbines smaller than 50 MW_{el} [21].

SUMMARY AND CONCLUSIONS

The fuel-flexibility of a LCV-combustor consisting of a FLOX® adopted main stage and a swirl stabilized pilot stage was analysed and demonstrated in this work by varying the hydrogen concentration in the fuel. Stable operation of the Turbec T100 was observed in all cases although the OH*-chemiluminescence and the OH-PLIF measurements showed different flame behaviour depending on high and low hydrogen contents. While the highest concentrations of OH radicals were found on the main stage nozzle axis for high hydrogen contents, they were located within the inner recirculation zone evenly distributed for $H_2 \leq 3\%$. This indicates a different flame stabilization mechanism depending on the hydrogen content, which strongly influences ignition delay times. Although the flames stabilise close to the orifices of the main stage nozzles for $H_2 = 30\%$, no flashback was observed. Efficient combustion was proved by exhaust gas analysis showing low emissions of carbon monoxide and nitrogen oxides.

The results demonstrate the ability of the LCV-combustor to operate with low calorific fuels containing hydrogen concentrations from 0 % to 30 %. Therefore, it enables reliable operation of the Turbec T100 with a high variety of LCV fuels as

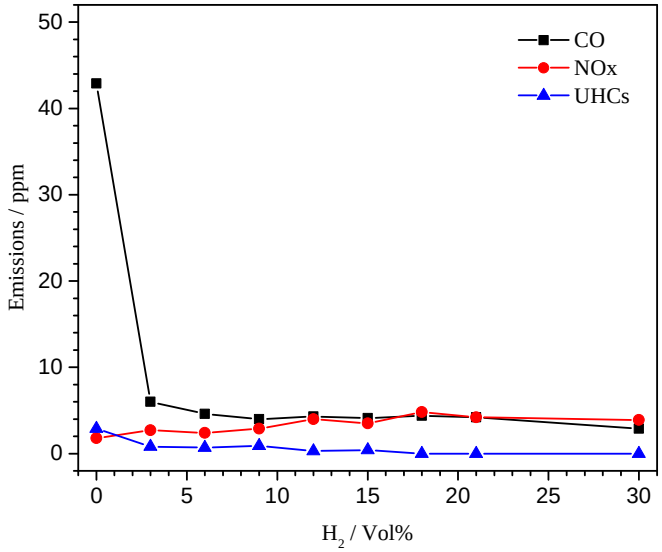

Fig. 10: POLLUTANT EMISSIONS BASED ON 15% O_2

well as the compliance with emission regulations. Till now, the combustor was only tested for product gases from biomass gasification. Beside the coupling of the micro gas turbine with a fixed-bed gasifier, the use in further applications is possible. As the position of the dilution holes and the length of the liner differed in the optical combustion chamber compared to the common design without optical access, emission performance should be investigated into detail if fuels with low hydrogen concentrations shall be used. The more lift-off position of the flame in that case may interfere with the dilution air, which could require design adaptation. Finally, this work contributes to a better understanding of FLOX® combustors by showing the different flame stabilization effects.

Acknowledgements

The authors want to thank Thomas Monz, Jan Zanger, Martin Stärk and Jochen Eichhorn for helping with the set-up and the operation of the test-rig. Trupti Kathrotia is thanked for the calculation of laminar flame speeds and ignition delay times. The German Federal Ministry for Economic Affairs and Energy is gratefully acknowledged for funding the project, in which this work was conducted.

References

[1] Pilavachi, P. A., 2000. "Power generation with gas turbine systems and combined heat and power". *Applied Thermal Engineering,* **20**, pp. 1421–1429.

[2] Carnö, J., Cavani, A., and Liinanki, L., 1998. "Micro gas turbine for combined heat and power in distributed generation". *ASME paper*(98-GT), p. 309.

[3] Gupta, K., Rehman, A., and Sarviya, R., 2010. "Bio-fuels for the gas turbine: A review". *Renewable and Sustainable Energy Reviews,* **14**(9), pp. 2946–2955.

[4] Hasler, P., Buehler, R., and Nussbaumer, T., 1998. "Evaluation of gas cleaning technologies for biomass gasification". In Biomass for Energy and Industry, 10th European Conference and Technology Exhibition; June8-11, Würzburg (Germany).

[5] Zornek, T., Monz, T., and Aigner, M., 2015. "Performance analysis of the micro gas turbine turbec t100 with a new flox-combustion system for low calorific fuels". *Applied Energy,* **159**, pp. 276–284.

[6] Wünning, J., and Wünning, J., 1997. "Flameless oxidation to reduce thermal no-formation". *Progress in Energy and Combustion Science,* **23**(1), pp. 81 – 94.

[7] Cavaliere, A., and Joannon, M., 2004. "Mild combustion". *Progress in Energy and Combustion Science,* **30**(4), pp. 329 – 366.

[8] Arghode, V., and Gupta, A. K., 2010. "Effect of flow field for colorless distributed combustion (cdc) for gas turbine combustion". *Applied Energy,* **87**, pp. 1631–1640.

[9] Tsuji, H., Gupta, A., Hasegawa, T., Katsuki, M., Kishimoto, K., and Morita, M., 2003. *High Temperature Air Combustion - From Energy Conservation to Pollution Reduction*. CRC Press, Florida.

[10] Lückerath, R., Meier, W., and Aigner, M., 2008. "Flox® combustion at high pressure with different fuel compositions". *Journal of Engineering for Gas Turbines and Power,* **130**(1), p. 011505.
[11] Schütz, H., Lückerath, R., Kretschmer, T., Noll, B., and Aigner, M., 2006. "Analysis of the pollutant formation in the flox combustion". In Proceedings of ASME Turbo Expo, no. GT2006-91041, Barcelona, Spain, May 8-11, 2006.
[12] Flamme, M., 2004. "New combustion systems for gas turbines (ngt)". *Applied Thermal Engineering,* **24**, pp. 1551–1559.
[13] Wünning, J., 2006. "Flameless combustion and its applications". *Natural Gas Technologies. Orlando (USA),* **30**.
[14] Zanger, J., Monz, T., and Aigner, M., 2015. "Experimental investigation of the combustion characteristics of a double-staged flox-based combustor on an atmospheric and a micro gas turbine test rig". In Proceedings of ASME Turbo Expo 2015, no. GT2015-42313, Montreal, Canada, June 15-19, 2015.
[15] Herzler, J., Herbst, J., Kick, T., Naumann, C., Braun-Unkhoff, M., and Riedel, U., 2013. "Alternative fuels based on biomass: An investigation of combustion properties of product gases". *Journal of Engineering for Gas Turbines and Power,* **135**(3), p. 031401.
[16] Huang, Z., Zhang, Y., Zeng, K., Liu, B., Wang, Q., and Jiang, D., 2006. "Measurements of laminar burning velocities for natural gas-hydrogen-air mixtures". *Combustion and Flame,* **146**, pp. 302–311.
[17] Li, J., Zhao, Z., Kazakov, A., Chaos, M., Dryer, F., and Scire, J., 2007. "A comprehensive kinetic mechanism for co, ch2o and ch3oh combustion". *International Journal of Chemical Kinetics,* **39**, pp. 109–136.
[18] Sadanandan, R., Stöhr, M., and Meier, W., 2008. "Simultaneous oh-plif and piv measurements in a gas turbine model combustor". *Applied Physics B,* **90**(3-4), pp. 609–618.
[19] Zanger, J., 2016. "Experimentelle charakterisierung eines atmosphrisch betriebenen, jet-stabilisierten mikrogasturbinenbrenners für erdgas". PhD thesis, Universitt Stuttgart.
[20] Borghi, R., 1985. "On the structure and morphology of turbulent premixed flames". In *Recent advances in the Aerospace Sciences*. Springer, pp. 117–138.
[21] Federal Ministry for Environment, Nature Conservation and Nuclear Safety, 2002. First general administrative regulation pertaining the federal immission control act (technical instructions on air qualitiy control - ta luft).